nature climate change

SUPPLEMENTARY INFORMATION

https://doi.org/10.1038/s41558-018-0245-3

In the format provided by the authors and unedited.

Detection of continental-scale intensification of hourly rainfall extremes

Selma B. Guerreiro[1*], Hayley J. Fowler[1], Renaud Barbero[1,2], Seth Westra[3], Geert Lenderink[4], Stephen Blenkinsop[1], Elizabeth Lewis[1] and Xiao-Feng Li[1]

[1]School of Engineering, Newcastle University, Newcastle, UK. [2]Irstea, Mediterranean Ecosystems and Risks, Aix-en-Provence, France. [3]School of Civil, Environmental and Mining Engineering, University of Adelaide, Adelaide, South Australia, Australia. [4]Royal Netherlands Meteorological Institute, De Bilt, The Netherlands. *e-mail: selma.guerreiro@ncl.ac.uk

Detection of continental-scale intensification of hourly rainfall extremes

Supplementary material

Contents

1 Quantiles and K-largest

Figure S.1 – a) daily and b) hourly range of different rainfall values associated with each K-largest value (the K-largest value itself not the bin mean). c) Quantile values associated with each K-largest value (the K-largest value itself not the bin mean). K-largest – quantile correspondence is almost the same for daily and hourly rainfall so only daily is shown. Boxplots show the spread of all gauges in the study for both periods of analysis 1966-1989 – period 1 in red and 1990-2013 – period 2 in blue (boxes show the interquartile range with the median, whiskers extend to 1.5 times the interquartile range and values above or below this are shown as dots).

2 Aerosols

Aerosols can have an impact on extreme rainfall by their influence on cloud microphysical processes that potentially lead to an invigoration of deep convective clouds [1]. For the city of Brisbane, aerosols have been shown to be associated with areas of less intense rain for stratiform systems, while for cumuliform systems, aerosols might be associated with enhanced rain downwind of the emissions [2]. However, Mitchell, Forgan [3] analysed aerosols in Australia for the period 1997-2015 using 22 stations spread across the country and found no widespread changes in aerosols (significant but small, negative trends were present in only four gauges).

Aerosols can also have a more widespread indirect effect by changing land-sea temperature contrasts, which in model simulations has been shown to affect the southern hemisphere ocean circulation [4]. Aerosols might also increase the tendency of monsoonal winds to flow toward Australia and make the tropical Pacific conditions similar to La Niña affecting mean seasonal rainfall in parts of Australia [5]. However, extreme rainfall and mean rainfall are not expected to show the same rates of change[6]. In this study we have shown that both daily and hourly extreme rainfall are increasing (at very different rates) against a background of strong regional patterns of changes in mean rainfall in Australia with severe recent drought in parts of south Australia while rainfall seems to be increasing in the north of Australia[7]. Therefore, since no literature could be found for large-scale impact of aerosols in extreme rainfall this could not be considered in our study.

3 Number of gauges used

Figure S.2 shows the sensitivity of our results to the number of gauges used in the study. The figure indicates the range of possible continental mean changes for daily and hourly rainfall extremes when using fewer gauges (25%, 50%, 75% and 99% of the gauges used in this study). When using only 25% of gauges (i.e. 27 gauges) the continental means vary widely (depending on which gauges are used) and can even be negative. It can be noted however, that even when using only 50% of gauges there are no negative changes for the hourly intensities.

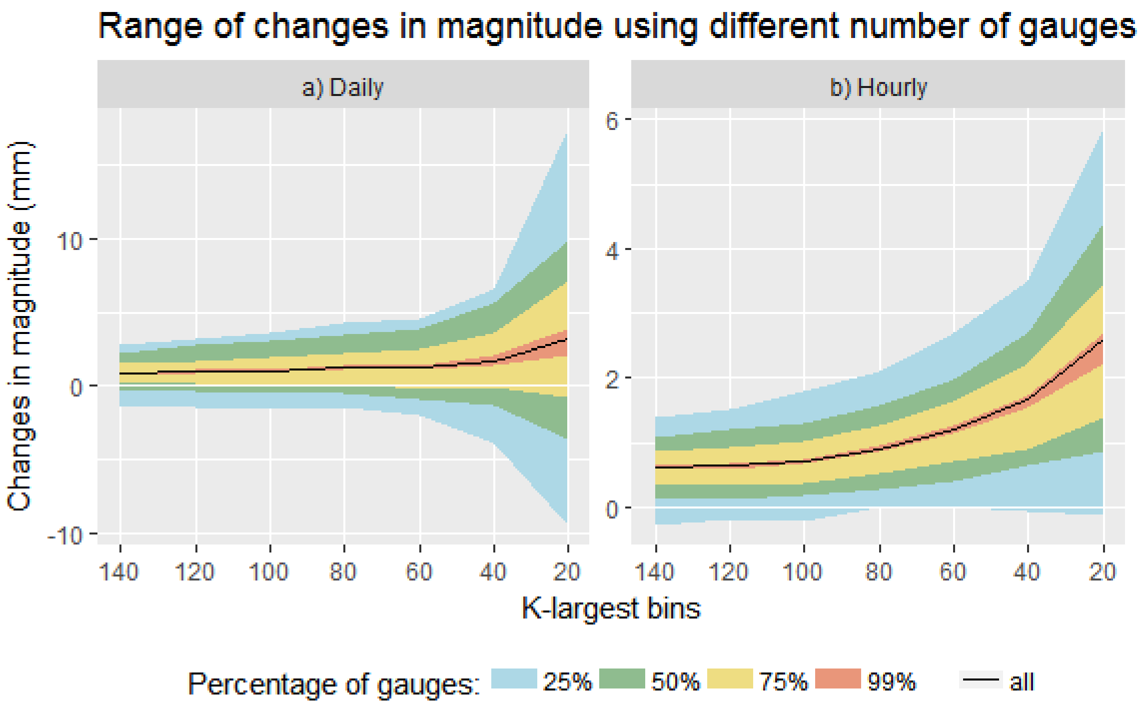

Figure S.2 – Impact of the number of gauges used to calculate changes in a) daily and b) hourly changes in the magnitude of extreme rainfall. Different colours show the range of possible results when using only 25%, 50%, 75% and 99% of the available gauges (calculations were performed using 10 000 permutations without repetition to illustrate possible combinations in gauge selection). The x-axis labels show the lower end of the bins.

4 Robustness of the method

The following plots show that the impact of methodological choices to our conclusions is negligible. Independently of how they are calculated (means or medians of the K-largest bins, absolute or relative changes per gauge, spatial means or medians of the Australian continent), continental changes in daily rainfall magnitudes are always around CC-scaling and within (or close to) the limits of changes expected from internal variability. Hourly changes are always well above what could be expected from internal variability and, for the higher values, well above 2xCC.

Bin mean – absolute changes (per gauge) – spatial mean

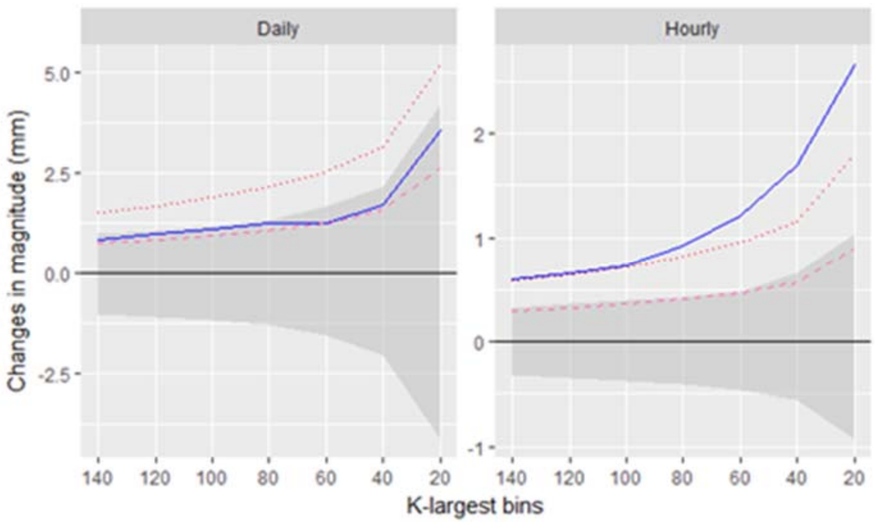

Bin median – absolute changes (per gauge) – spatial mean

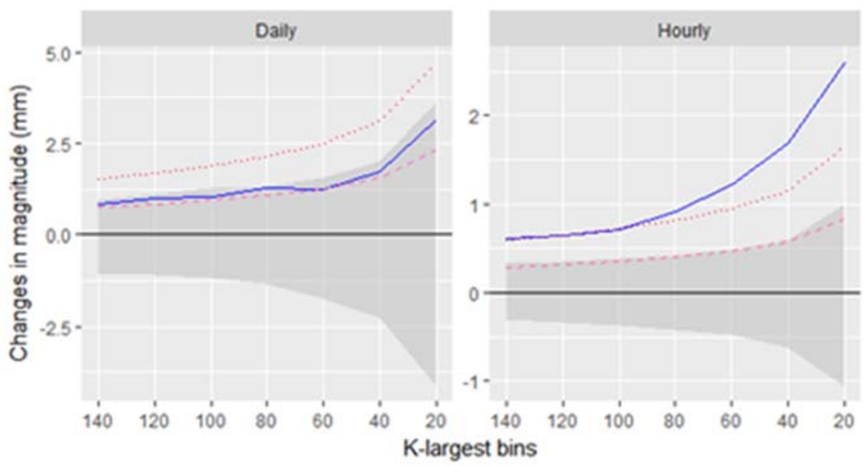

Bin median – absolute changes (per gauge) – spatial median

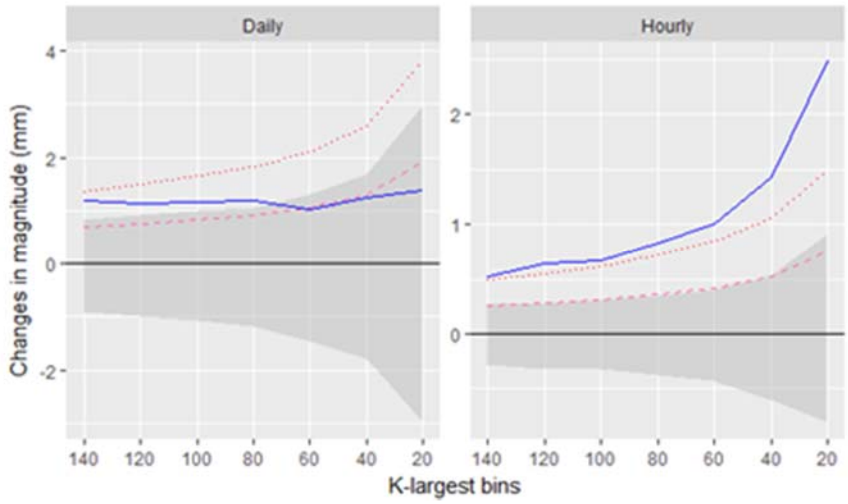

Bin median – relative changes (per gauge) – spatial median

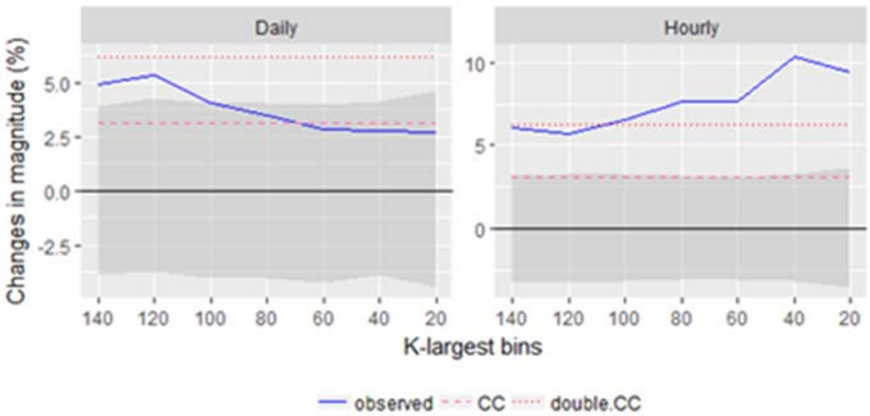

Figure S.3 – Changes (differences) in magnitude (in mm or %) of daily (left) and hourly (right) K-largest values for: observations (solid blue line), expected changes based on the Clausius-Clapeyron (CC) scaling (dashed red line) and double the expected changes based on CC-scaling (2xCC - dotted red line). The shaded grey area shows the changes expected due to internal variability using a 99th confidence interval (calculated using a bootstrapping technique on the observed dataset, i.e. time-series were randomly reshuffled, with replacement and retaining spatial correlation, and then divided into two sub-periods and changes calculated: the procedure was repeated 1000 times). All changes are shown as spatial means or medians of 107 gauge records across Australia between 1990-2013 and 1966-1989. The x-axis labels show the lower end of the bins (i.e. K-largest 20 – K20 – shows the mean or median change of the 20 largest values, K40 shows the mean or the median change of the values K21 to K40 inclusive, etc.)

5 Temperature and change factor calculation

In this study, we used global mean surface temperature (GMST) from GISS [8, 9] to determine the change in GMST between the 1966-1989 and 1990-2013 periods. We then used this information together with a CC-scaling rate of 6.5 % °C^{-1} to calculate rainfall change factors (CFs) to apply to rainfall from the first period to estimate the change we would expect with CC and 2xCC scaling. However, we also investigated how the results would differ with the use of different estimates of temperature change. Since the drivers of rainfall in Australia can be remote [10, 11], changes in mean surface temperature over different geographical areas were used to calculate rainfall CFs (Figure S.4). We present these different estimates of temperature change and their respective CFs in Table S.1. A different dataset (HadCRUT4 [12]) was also used to assess the impact of the choice of temperature dataset.

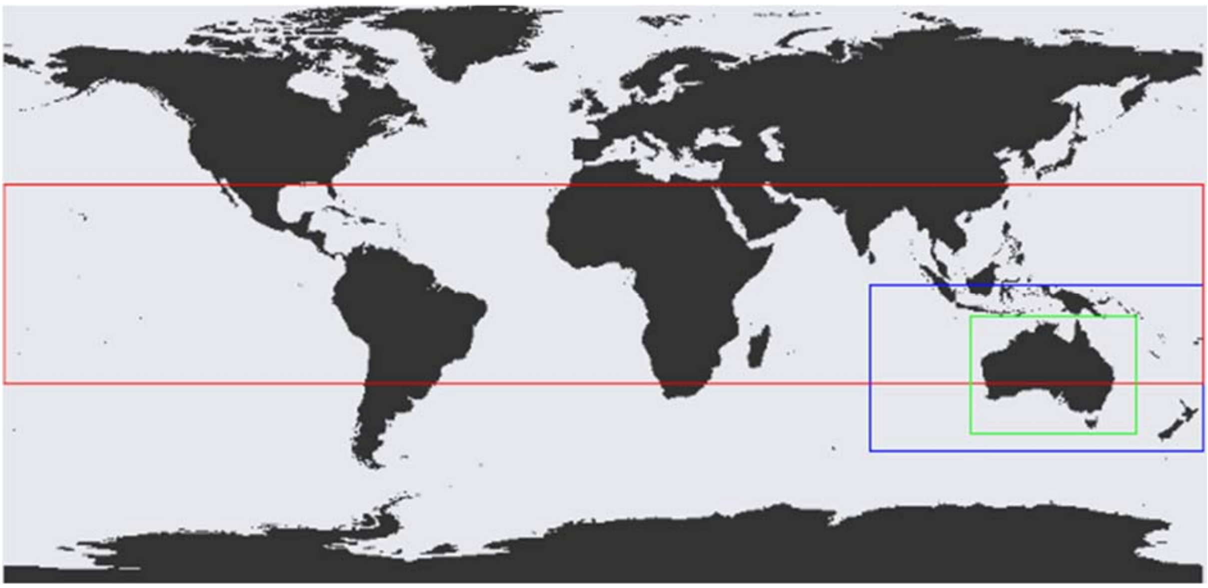

Figure S.4 – Alternative areas for calculation of temperature changes – Tropics (red), Australasia (blue) and Australia (green).

Table S.1 Changes in mean surface temperature between 1966-1986 and 1987-2013 and respective change factor (based on CC-rate of 6.5% °C^{-1}) for different regions for two different datasets: GISS Surface Temperature Analysis (Land-Ocean Temperature Index, ERSSTv5)[8, 9] and HadCRUT4 (global historical surface temperature anomalies) [12].

	GISTEMP	HadCRUT4
Global	0.48°C CF=1.031*	0.43°C CF=1.028
Tropics Lat=[-30,30]	0.36°C CF=1.023	0.34°C CF=1.022
Australasia Lat = [-50,0] Lon = [80,180]	0.33°C CF=1.021	0.31°C CF=1.020
Australia Lat = [-45,-10] Lon = [110,1660]	0.34°C CF=1.022	0.34°C CF=1.022

* CF = 1+(0.48x0.065)=1.0312

Since the temperature dataset used in this study (Global GISTEMP) shows the higher CF, the results of the study would be strengthened by the use of temperature from another geographical area/dataset. To illustrate this, Figure S.5 shows changes in the magnitude of extreme rainfall with the expected changes calculated using the Australasian area shown in Figure S.4 and the CRU dataset (i.e. the lowest CF). The behaviour is similar to that shown in Figure 1 in the main paper but the changes in daily extremes are now closer to 2xCC, while the changes in hourly extremes are always more than 2xCC.

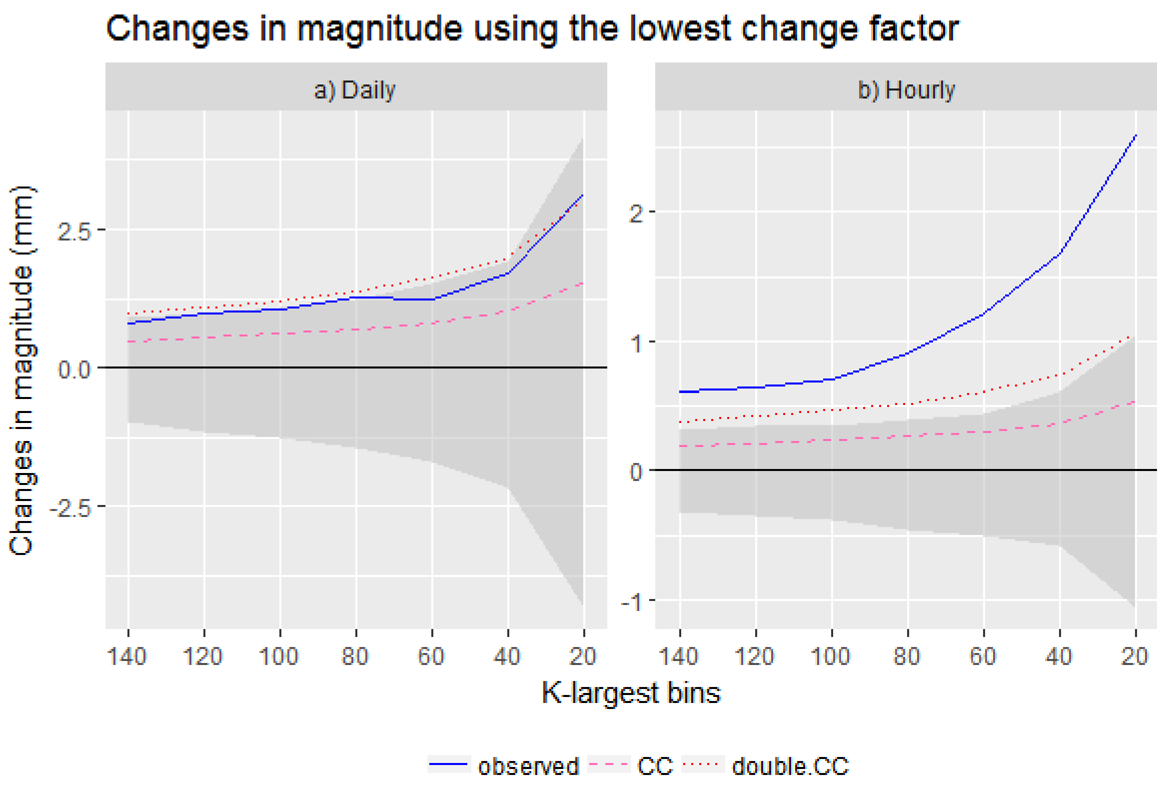

Figure S.5 – Changes (differences) in magnitude (in mm) of daily (left) and hourly (right) K-largest values for: observations (solid blue line), expected changes based on Clausius-Clapeyron (CC) scaling (dashed red line) and double the expected changes based on CC-scaling (2xCC, dotted red line). The temperature used for the CC scaling was calculated using the area encompassed by the Australasian box (Figure S.4 - latitude between 50°S and 0° and longitude between 80°E and 180°E) which shows the smallest change in temperature of all areas assessed. The shaded grey area shows the changes expected due to internal variability using a 99th confidence interval (calculated using a bootstrapping technique on the observed dataset, i.e. time-series were randomly reshuffled, with replacement and keeping spatial correlation, and then divided into two sub-periods and changes calculated, the procedure was repeated 1000 times). All changes are shown as spatial means of Australia between 1990-2013 and 1966-1989. The x-axis labels show the lower end of the bins (i.e. K-largest 20 – K20 – shows the mean change of the 20 largest values, K40 shows the mean change of the values K21 to K40 inclusive).

6 Frequency changes

Since changes in rainfall magnitude should result in frequency changes, we also assessed the continental mean changes in the frequency of values above each K-largest. Changes to the frequency of daily and hourly rainfall extremes are shown in Figure S.6 for K-largest values calculated for Period 1: 1966-1989 (see "Data & Methods"). We find that continental-scale changes scale at CC or sub-CC for daily extremes and are well within the range expected from internal variability. However, the change in hourly extreme rainfall frequencies scales at between CC to 2xCC for the most extreme intensities, and frequency changes for >K120 are outside the range expected from natural variability.

To assess possible out-of-sample problems[13, 14] (i.e. impact of the K-largest being calculated on period 1 and applied to period 2), Figure S.7 shows the results using Period 2 (1990-2013) and the whole record (1966-2013) to calculate K-largest values. Although the absolute changes differ with the period chosen to define the K-largest, the behaviour is similar, with daily changes always being below CC and hourly changes around 2xCC for K20. The largest difference is that using all data to define the K-largest the changes in hourly extremes are always well above CC-scaling (even for the lower extremes).

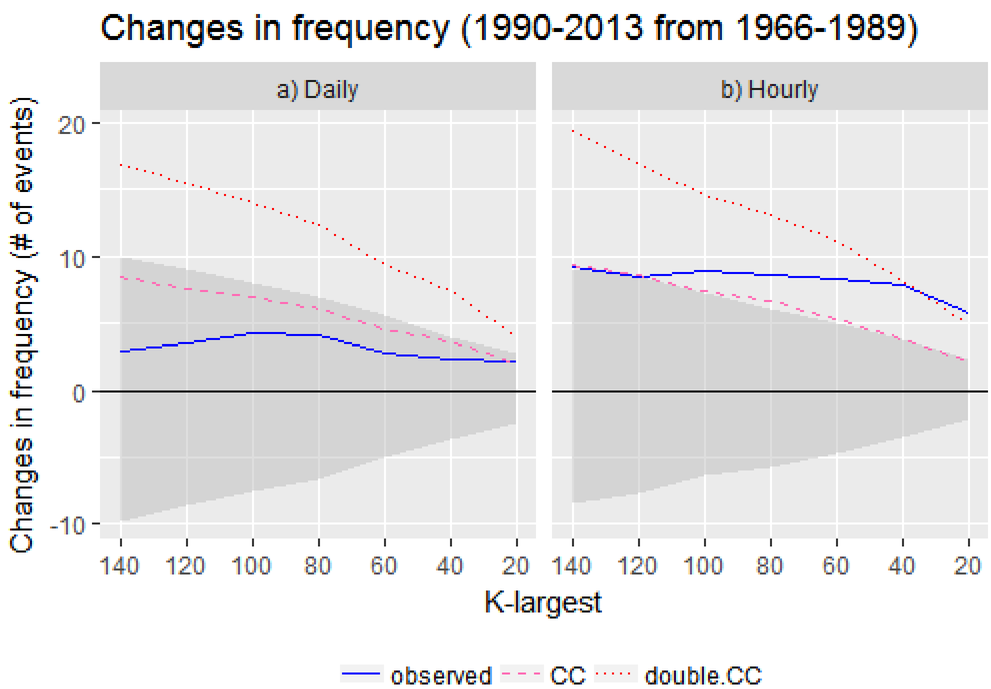

Figure S.6 – Changes (difference) in number of daily (left) and hourly (right) K-largest values for: observations (solid blue line), expected changes based on Clausius-Clapeyron (CC) scaling (dashed red line) and double the expected changes based on CC-scaling (2xCC, dotted red line). The shaded grey area shows the changes expected due to internal variability using a 99th confidence interval (calculated using a bootstrapping technique on the observed dataset, i.e. time-series were randomly reshuffled, with replacement and keeping spatial correlation and then divided into two sub-period and changes calculated, the procedure was repeated 1000 times). All changes are shown as spatial means of changes for 107 gauges across Australia between 1990-2013 and 1966-1989. The x-axis labels show the lower end of the bins (i.e. K-largest 20 shows the change in the number of values equal to or above the magnitude of the 20th largest value of the first period).

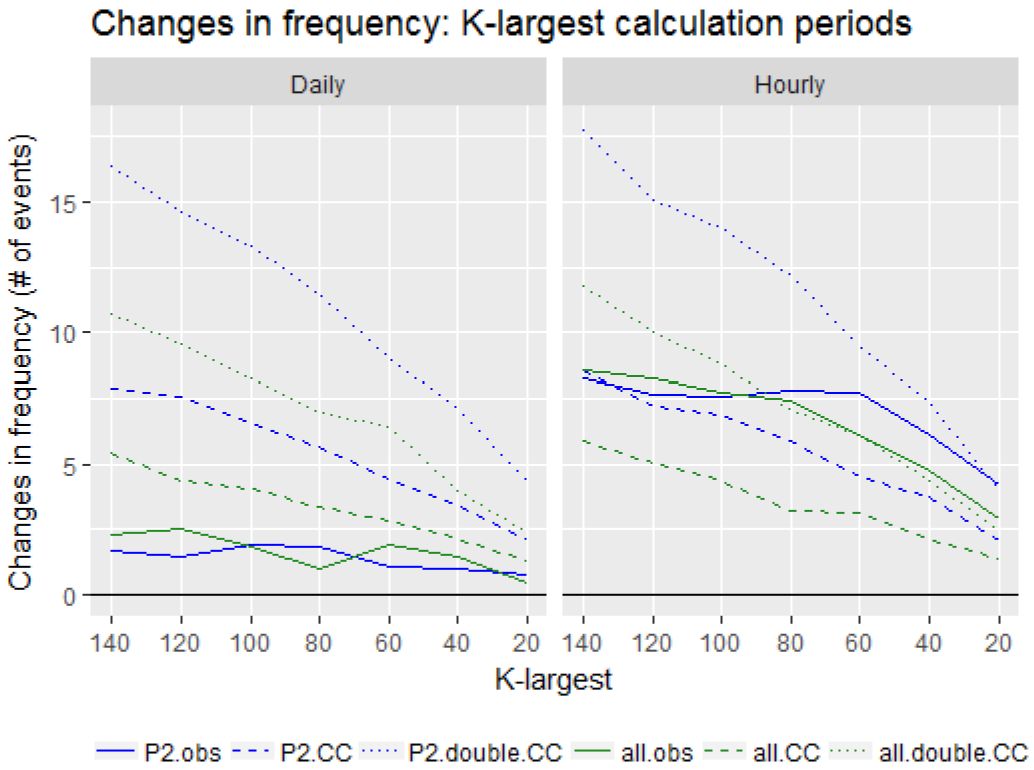

Figure S.7 – Changes in the frequency of daily (left) and hourly (right) K-largest values for: observations (solid lines), expected changes based on Clausius-Clapeyron (CC) scaling (dashed lines) and double the expected changes based on CC-scaling (2xCC, dotted lines). K-largest values were calculated using the second period - 1990-2013 ("P2" - blue) and using the whole dataset – 1966-2013 ("all" - green). All changes are shown as spatial means of changes at 107 gauges across Australia between 1990-2013 and 1966-1989. The x-axis labels show the lower end of the K-largest bins.

7 Seasonality

Shifts in seasonality of extreme events could affect our results if extreme events that tended to happen in the cooler season became more prevalent in the warmer season. A possible change in seasonality of extremes could therefore have a stronger impact than the direct role of thermodynamic effects due to the rise of the global mean temperature. Since Australia has very different climatic zones, from tropical to desert to temperate, there are no coherent seasons that can be applied to all regions. Therefore, "seasonality" was analysed by looking at which months the intense rainfall occurred in. To assess possible changes in seasonality, we selected the 20 highest values per gauge and, for each gauge, we calculated the modal month of extreme values (the month with higher occurrences of extreme values). To investigate if extremes are spread around the year or clustered in the modal month we calculated the Gini coefficient [15] using the R-package "ineq"[16]. This coefficient is commonly used as a summary measure of income inequality but has also been used in hydroclimatic studies[17, 18]. The Gini coefficient is defined as the mean absolute difference between all pairs of items of a population - in this case all pairs of monthly frequencies of values above K20 (for each gauge).

The coefficient ranges from zero (if all months have the same number of values above K20) to one (if one month has all the values above K20).

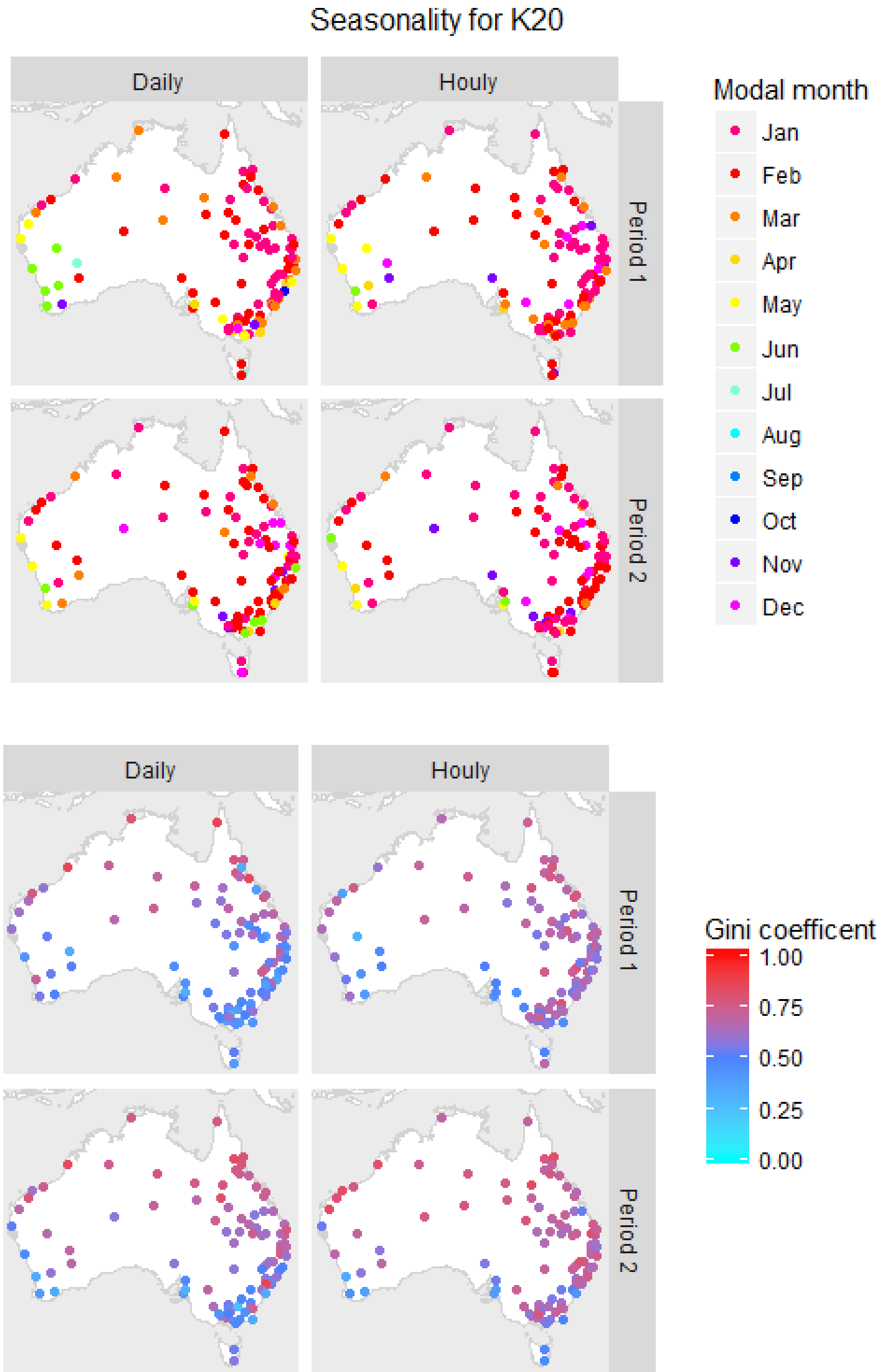

Figure S.8 – Seasonality of the 20 largest values per gauge. The top four maps show the modal month of extreme values (month with higher number of rainfall values equal or above K20) for daily and hourly rainfall and for period 1 (1966-1989) and period 2 (1990-2013). The lower four maps show the Gini coefficient - a measure of the spread of the extreme events across the months of the year.

Figure S.8 shows that, for both daily and hourly rainfall, the biggest 20 values tend to occur in December to March (Austral summer) for both periods of analysis. The only exception is the West coast where a few gauges show most of the extreme values during April-June. The Gini coefficient ranges from 0.2 to 0.9 with the higher values present in the north of Australia where the extremes tend to gather more strongly around the same month. The lowest values are in the south of Australia, especially for daily rainfall where the extreme values are more spread across different months. Not surprisingly, this is also the area where more gauges show a different modal month between the two periods of analysis for daily rainfall since the seasonality of extremes is relatively week and therefore differences are likely to be due to sampling/internal variability.

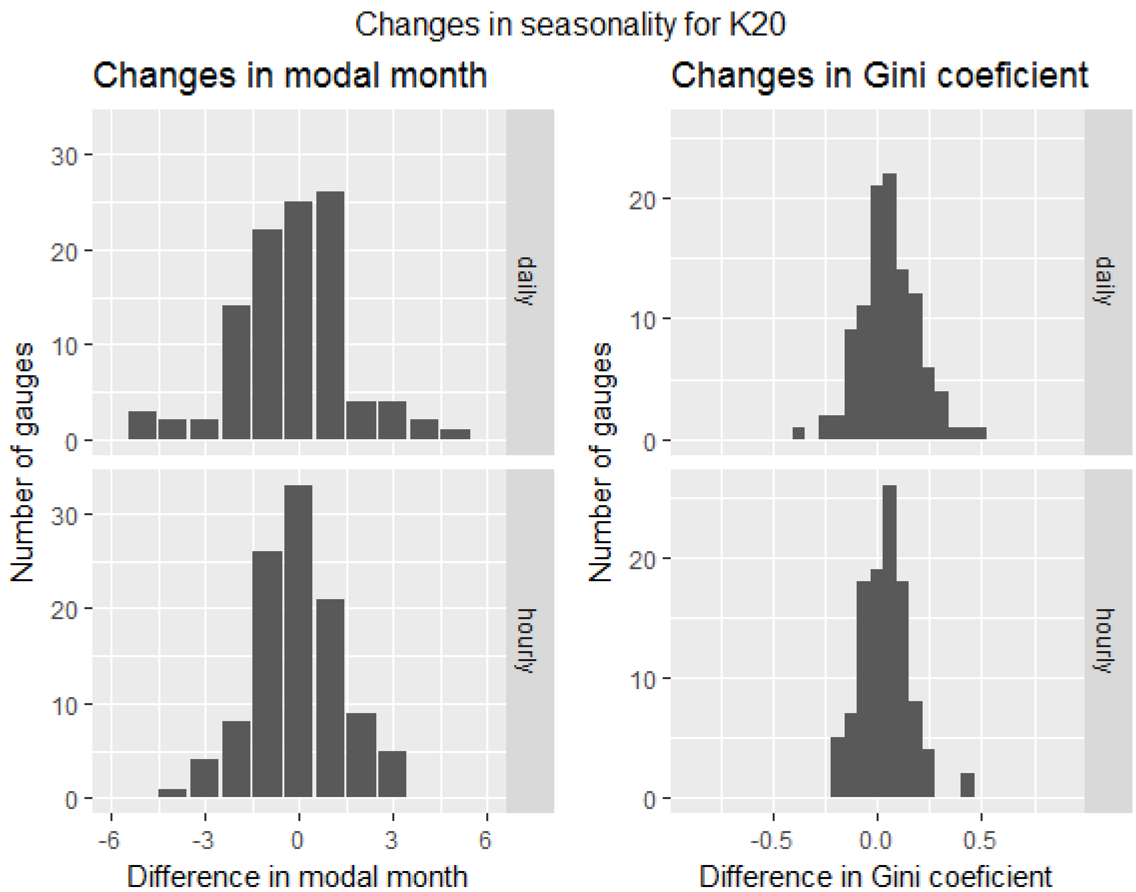

Figure S.9 – Changes in modal month (of the 20 largest rainfall values) per gauge for daily (top) and hourly (bottom) rainfall between period 1 (1966-1989) and period 2 (1990-2013). Positive values mean the modal month in period 2 is after period 1, negative values show the reverse (so for example if the modal month changes from February to April the difference would be 2 while February to December would be -2).

Examining changes in the modal month between the two periods (*Figure S.9*, left) it is clear that in most gauges the modal month is not changing or is changing by just 1 (2) month(s) for hourly (daily) rainfall. Furthermore, the Gini coefficient is also not changing much between the two periods; for hourly rainfall, 75% of gauges have changes in the Gini coefficient between -0.02 and 0.1. Therefore, there is also no noteworthy change in the strength of the seasonality.

We therefore concluded that: most gauges have extreme values occurring predominantly in the warm months for both periods, changes in the modal month are restricted to 1 or 2 months for most gauges and the strength of seasonality has not substantially changed in-between the two periods of analysis. Consequently, changes in seasonality of precipitation extremes does not impact our results.

8 ENSO variability

Figure S.10 shows the El Niño Southern Oscillation (ENSO) Niño 3.4 index time-series[19] for the period of analysis and Table S.2 indicates the number of months in each phase (El Niño, La Niña or neutral).

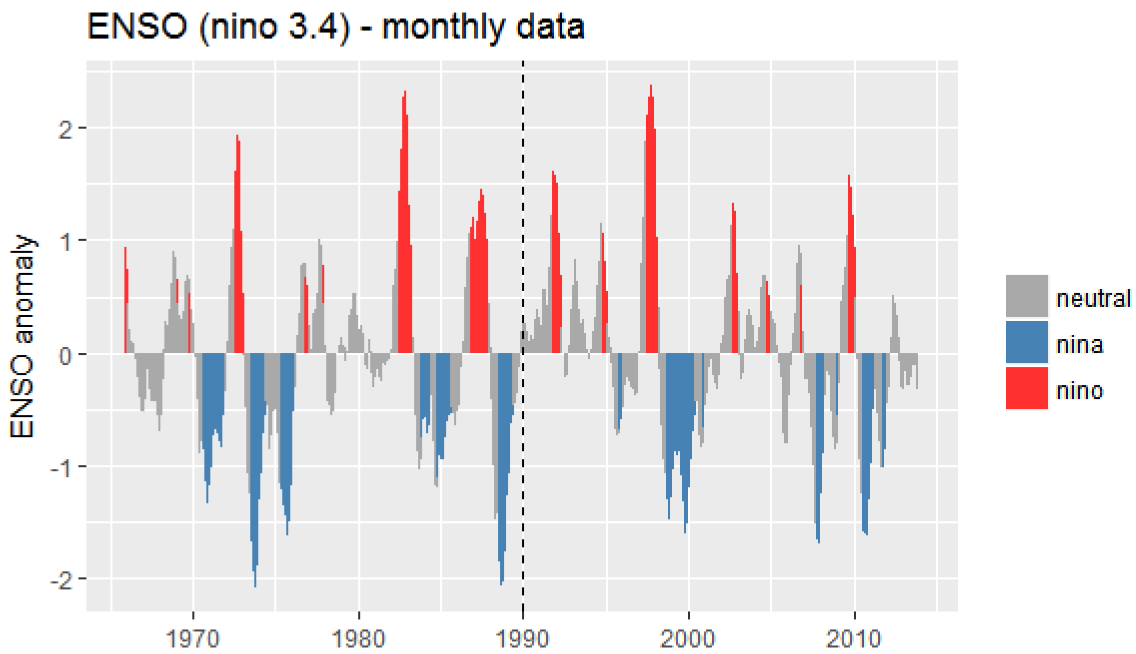

Figure S.10 – Niño 3.4 index time series[19] with La Niña phases shown in blue and El Niño phases in red. The two periods of analysis are separated by the dashed black line.

Table S.2 – Number of months in El Niño, La Niña and Neutral phases for the three periods of analysis.

	1966-1989	1990-2013	1966-2013
El Niño	36	29	65
La Niña	63	42	105
Neutral	189	217	406

Figure S.11 shows the spatial patterns of the effect of ENSO's phase on the occurrence of hourly extremes (K20, K40 and K60).

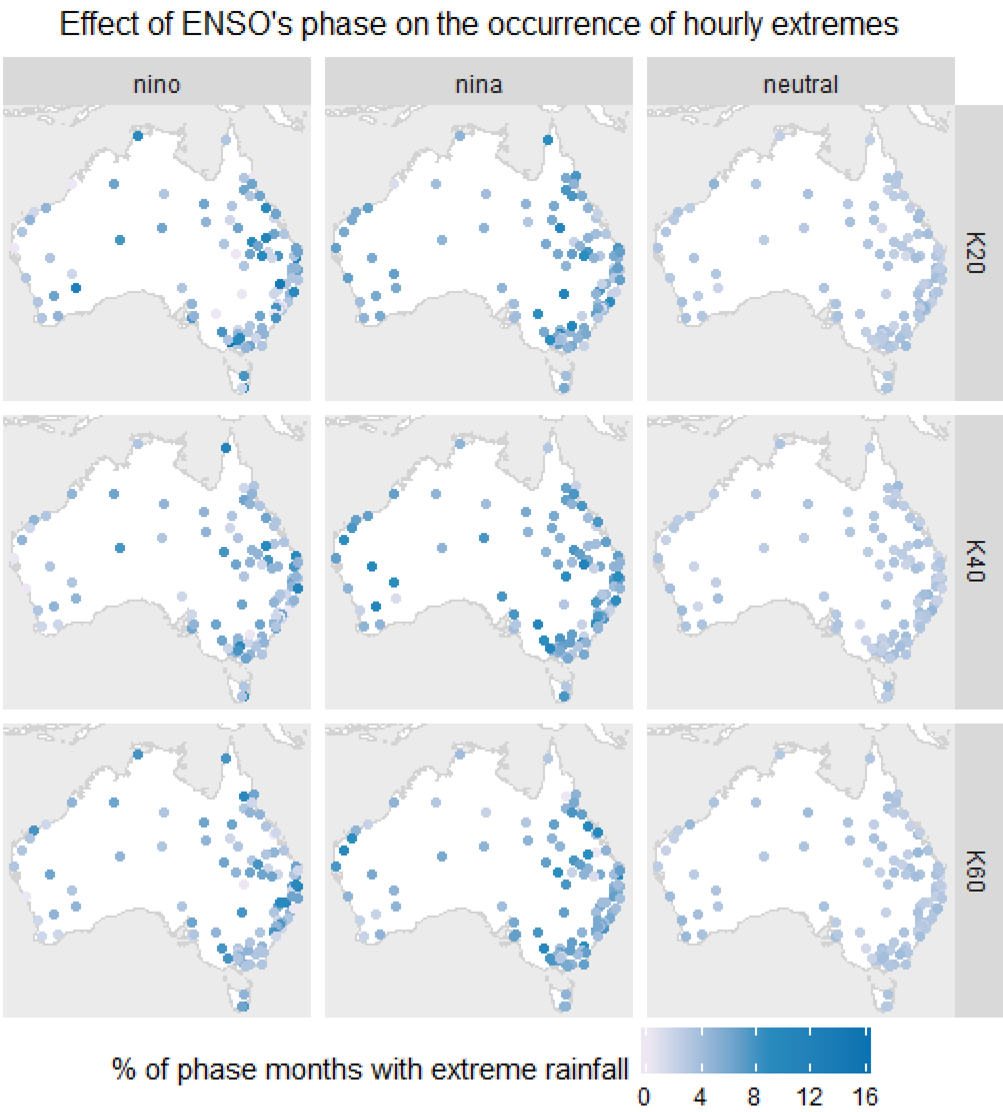

Figure S.11 – Percentage of El Niño, La Niña and neutral months with extreme hourly rainfall, for different K-largest bins. The labels show the lower end of the bins; K20 – shows the percentage of nino/nina/neutral months with values above or equal to K20, K40 shows the percentage of months with values between K40 (inclusive) and K20 (exclusive) and K60 between K60 and K40.

Changes in the Niño 3.4 index time series between 1966 and 2013 were assessed using the Pettitt test (change point analysis) and the Mann-Kendall test (trend analysis). Null hypothesis significance tests assume data is independent and identically distributed while Niño 3.4 index shows strong autocorrelation. Therefore, the significance of the tests was calculated by comparing observed test statistics with the test statistics for 100,000 surrogate Niño 3.4 indices. The surrogates are random time-series with the same distribution and autocorrelation but stationary, created using iterated amplitude adjusted Fourier transformations [20, 21, 22, 23]. The variance was calculated as the squared residuals by fitting the time series with a locally weighted scatterplot smoothing (LOESS) function [24, 25, 26]. The results are presented in Figure S.12 to Figure S.15 showing that during the analysis period (1966-2013), we found no evidence for change points or trends within the Niño 3.4 index series or in its variance.

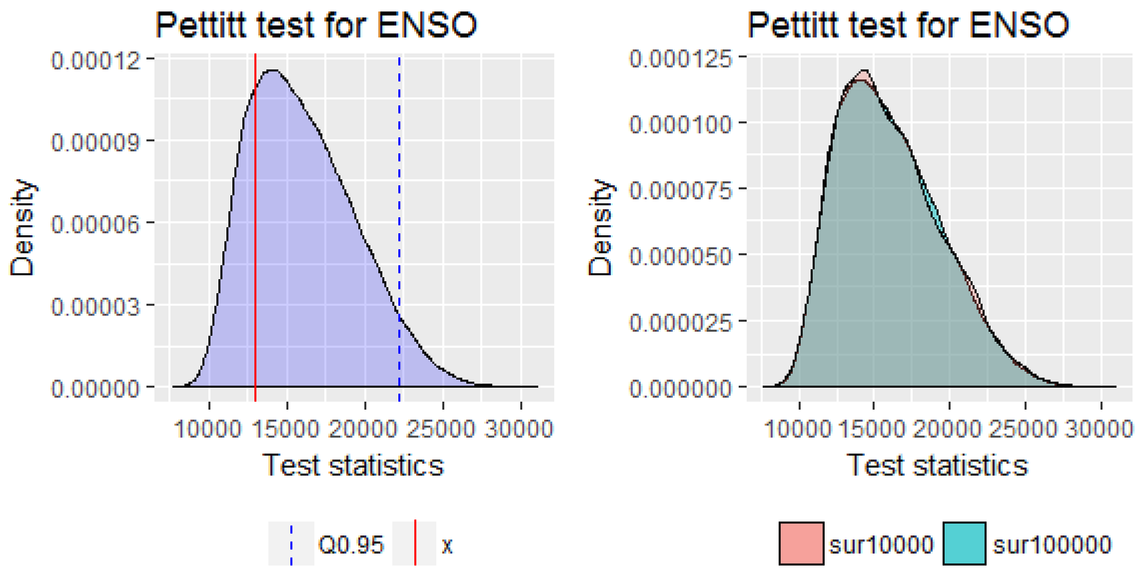

Figure S.12 – Change point analysis for ENSO (Niño 3.4 index) time series between 1966 and 2013 using the Pettitt test. The plot on the left shows the result for the observed series (x, red line) is below the 0.95 quantile of the surrogate series meaning no statistically significant change point was detected at the 0.05 significance level. The plot on the right shows the distribution of the results of the test statistics using 10 000 and 100 000 surrogates (sur) – since their distributions are almost identical, 100 000 surrogates were considered enough to perform the analysis.

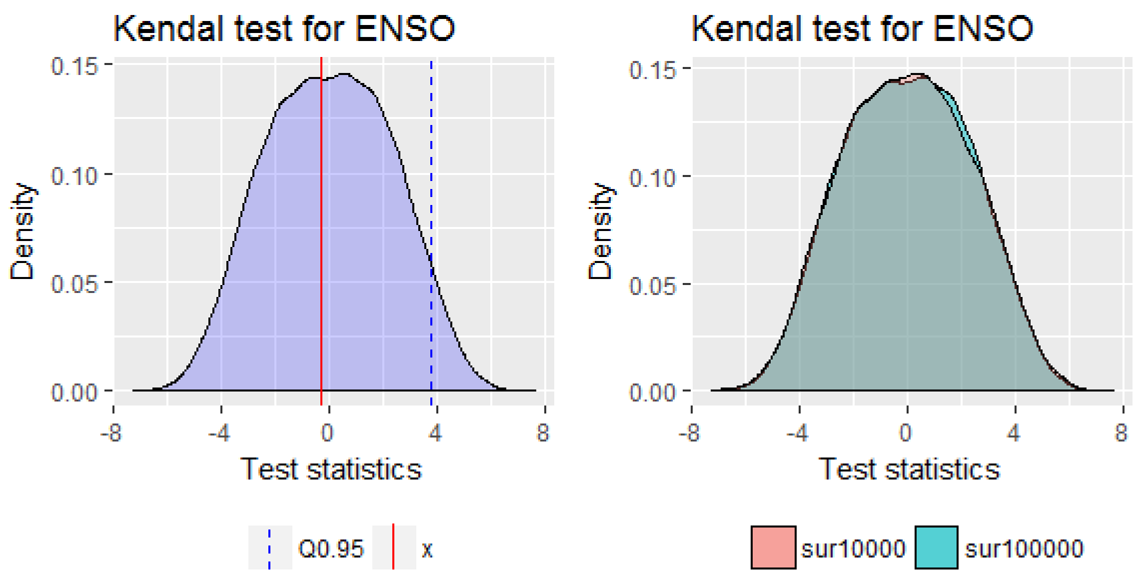

Figure S.13 – Trend analysis for ENSO (Niño 3.4 index) time series between 1966 and 2013 using the Mann-Kendall test. The plot on the left shows the result for the observed series (x, red line) is below the 0.95 quantile of the surrogate series meaning no statistically significant trend was detected at the 0.05 significance level. The plot on the right shows the distribution of the results of the test statistics using 10 000 and 100 000 surrogates (sur)– since their distributions are almost identical, 100 000 surrogates were considered enough to perform the analysis.

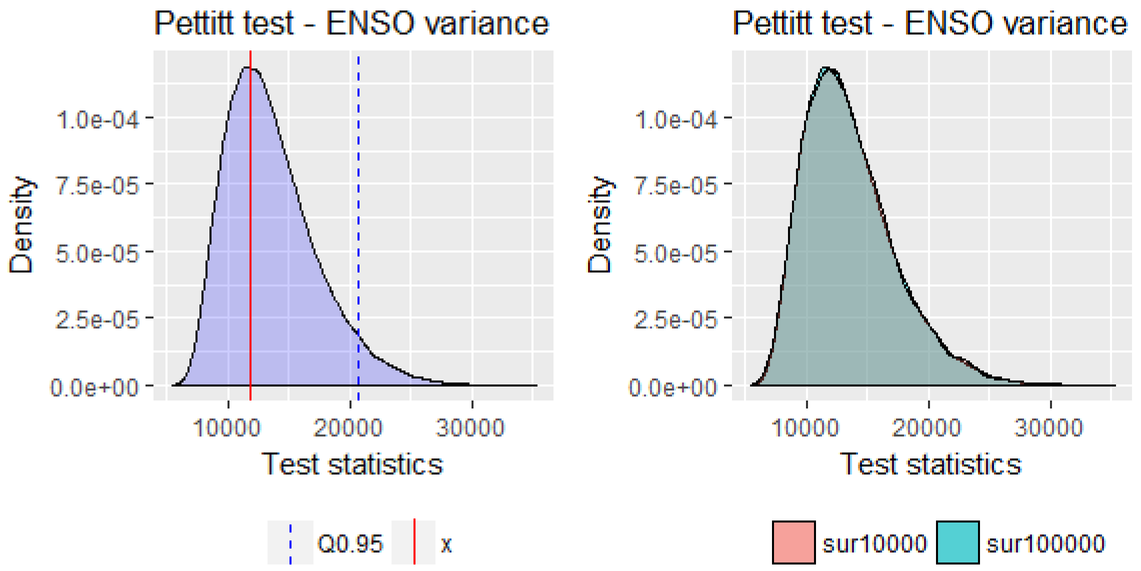

Figure S.14 – Change point analysis for ENSO's (Niño 3.4 index) variance time series between 1966 and 2013 using the Pettitt test. The plot on the left shows the result for the observed series (x, red line) is below the 0.95 quantile of the surrogate series meaning no statistically significant change point was detected at the 0.05 significance level. The plot on the right shows the distribution of the results of the test statistics using 10 000 and 100 000 surrogates (sur) – since their distributions are almost identical 100 000 surrogates were considered enough to perform the analysis.

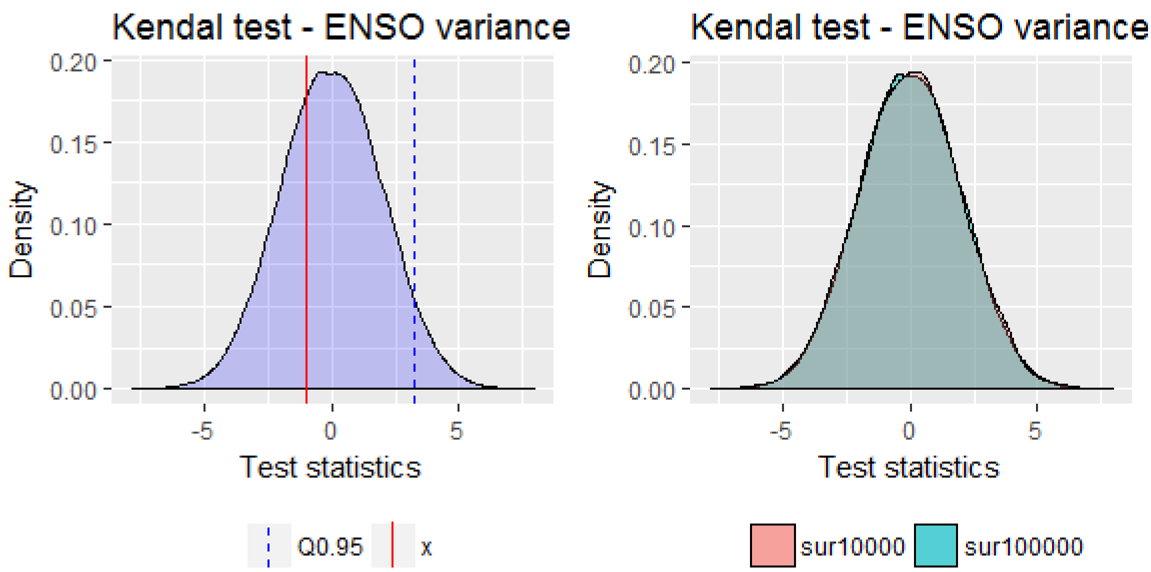

Figure S.15 – Trend analysis for ENSO's (Niño 3.4 index) variance time series between 1966 and 2013 using the Mann-Kendall test. The plot on the left shows the result for the observed series (x, red line) is below the 0.95 quantile of the surrogate series meaning no statistically significant trend was detected at the 0.05 significance level. The plot on the right shows the distribution of the results of the test statistics using 10 000 and 100 000 surrogates (sur) – since their distributions are almost identical 100 000 surrogates were considered enough to perform the analysis.

9 Supplementary Information References

1.Fan J, Rosenfeld D, Zhang Y, Giangrande SE, Li Z, Machado LAT*, et al.* Substantial convection and precipitation enhancements by ultrafine aerosol particles. *Science* 2018, **359**(6374)**:** 411-418.

2.Hewson M, McGowan H, Phinn S, Peckham S, Grell G. Exploring Aerosol Effects on Rainfall for Brisbane, Australia. *Climate* 2013, **1**(3)**:** 120.

3.Mitchell RM, Forgan BW, Campbell SK. The Climatology of Australian Aerosol. *Atmos Chem Phys* 2017, **17**(8)**:** 5131-5154.

4.Cai W, Cowan T. Impacts of increasing anthropogenic aerosols on the atmospheric circulation trends of the Southern Hemisphere: An air-sea positive feedback. *Geophysical Research Letters* 2007, **34**(23).

5.Rotstayn LD, Cai W, Dix MR, Farquhar GD, Feng Y, Ginoux P*, et al.* Have Australian rainfall and cloudiness increased due to the remote effects of Asian anthropogenic aerosols? *Journal of Geophysical Research: Atmospheres* 2007, **112**(D9).

6.Pendergrass AG. What precipitation is extreme? *Science* 2018, **360**(6393)**:** 1072-1073.

7.CSIRO and Bureau of Meteorology. Climate Change in Australia - Projections for Australia's Natural Resource Management Regions (Chapter 4 - Understanding Recent Australian Climate); 2015.

8.GISTEMP Team. ISS Surface Temperature Analysis (GISTEMP). NASA Goddard Institute for Space Studies. 2017 [cited 10-10-2017]Available from: https://data.giss.nasa.gov/gistemp/.

9.Hanson S, Nicholls R, Ranger N, Hallegatte S, Corfee-Morlot J, Herweijer C*, et al.* A global ranking of port cities with high exposure to climate extremes. *Climatic Change* 2011, **104**(1)**:** 89-111.

10.Risbey JS, Pook MJ, McIntosh PC, Wheeler MC, Hendon HH. On the Remote Drivers of Rainfall Variability in Australia. *Monthly Weather Review* 2009, **137**(10)**:** 3233-3253.

11.Xiao-Feng L, Jingjing Y, Yun L. Recent Summer Rainfall Increase and Surface Cooling over Northern Australia since the Late 1970s: A Response to Warming in the Tropical Western Pacific. *Journal of Climate* 2013, **26**(18)**:** 7221-7239.

12.Climatic Research Unit - University of East Anglia. HadCRUT4. 2017 [cited 10-10-2017]Available from: https://crudata.uea.ac.uk/cru/data/temperature/

13.Fischer EM, Knutti R. Observed heavy precipitation increase confirms theory and early models. *Nature Clim Change* 2016, **6**(11)**:** 986-991.

14.Xuebin Z, Gabriele H, Francis WZ, Jesse K. Avoiding Inhomogeneity in Percentile-Based Indices of Temperature Extremes. *Journal of Climate* 2005, **18**(11)**:** 1641-1651.

15.Gini C. Variabilità e mutabilità. In: Pizetti, E. and Salvemini, T. Eds., Rome: Libreria Eredi Virgilio Veschi, Memorie di metodologica statistica. 1912.

16.Zeileis A. ineq: Measuring Inequality, Concentration, and Poverty. R package version 0.2-13. https://CRAN.R-project.org/package=ineq; 2014.

17.Rajah K, O'Leary T, Turner A, Petrakis G, Leonard M, Westra S. Changes to the temporal distribution of daily precipitation. *Geophysical Research Letters* 2014, **41**(24)**:** 8887-8894.

18.Masaki Y, Hanasaki N, Takahashi K, Hijioka Y. Global-scale analysis on future changes in flow regimes using Gini and Lorenz asymmetry coefficients. *Water Resources Research* 2014, **50**(5)**:** 4054-4078.

19.Rayner NA, Parker DE, Horton EB, Folland CK, Alexander LV, Rowell DP*, et al.* Global analyses of sea surface temperature, sea ice, and night marine air temperature since the late nineteenth century. *Journal of Geophysical Research: Atmospheres* 2003, **108**(D14)**:** n/a-n/a.

20.Franzke C. A novel method to test for significant trends in extreme values in serially dependent time series. *Geophysical Research Letters* 2013, **40**(7)**:** 1391-1395.

21.Schreiber T, Schmitz A. Improved Surrogate Data for Nonlinearity Tests. *Physical Review Letters* 1996, **77**(4)**:** 635-638.

22.Schreiber T, Schmitz A. Surrogate time series. *Physica D: Nonlinear Phenomena* 2000, **142**(3)**:** 346-382.

23.Serinaldi F, Kilsby CG, Lombardo F. Untenable nonstationarity: An assessment of the fitness for purpose of trend tests in hydrology. *Advances in Water Resources* 2018, **111**(Supplement C)**:** 132-155.

24.Villarini G, Smith JA, Baeck ML, Vitolo R, Stephenson DB, Krajewski WF. On the frequency of heavy rainfall for the Midwest of the United States. *Journal of Hydrology* 2011, **400**(1-2)**:** 103-120.

25.Villarini G, Serinaldi F, Smith J, Krajewski W. On the stationarity of annual flood peaks in the continental United States during the 20th century. *Water Resources Research* 2009, **45**.

26.Guerreiro SB, Kilsby C, Serinaldi F. Analysis of time variation of rainfall in transnational basins in Iberia: Abrupt changes or trends? *International Journal of Climatology* 2014, **34**(1)**:** 114-133.